IOP Publishing Physical Biology
Phys. Biol. 11 (2014) 046001 (17pp) doi:10.1088/1478-3975/11/4/046001

Effects of microtubule mechanics on hydrolysis and catastrophes

N Müller and J Kierfeld

Department of Physics, TU Dortmund University, D-44221 Dortmund, Germany

E-mail: nina2.mueller@tu-dortmund.de and jan.kierfeld@tu-dortmund.de

Received 27 January 2014, revised 8 May 2014
Accepted for publication 12 May 2014
Published 4 June 2014

Abstract

We introduce a model for microtubule (MT) mechanics containing lateral bonds between dimers in neighboring protofilaments, bending rigidity of dimers, and repulsive interactions between protofilaments modeling steric constraints to investigate the influence of mechanical forces on hydrolysis and catastrophes. We use the allosteric dimer model, where tubulin dimers are characterized by an equilibrium bending angle, which changes from 0° to 22° by hydrolysis of a dimer. This also affects the lateral interaction and bending energies and, thus, the mechanical equilibrium state of the MT. As hydrolysis gives rise to conformational changes in dimers, mechanical forces also influence the hydrolysis rates by mechanical energy changes modulating the hydrolysis rate. The interaction via the MT mechanics then gives rise to correlation effects in the hydrolysis dynamics, which have not been taken into account before. Assuming a dominant influence of mechanical energies on hydrolysis rates, we investigate the most probable hydrolysis pathways both for vectorial and random hydrolysis. Investigating the stability with respect to lateral bond rupture, we identify initiation configurations for catastrophes along the hydrolysis pathways and values for a lateral bond rupture force. If we allow for rupturing of lateral bonds between dimers in neighboring protofilaments above this threshold force, our model exhibits avalanche-like catastrophe events.

Keywords: microtubules, dynamic instability, hydrolysis, catastrophes

1. Introduction

Microtubule (MT) dynamics is essential for many cellular processes, such as cell division [1], intracellular positioning processes [2], e.g. positioning of the cell nucleus [3] or chromosomes during mitosis, establishing cell polarity [4], or regulation of cell shapes [5, 6]. An important feature of MT dynamics is their dynamic instability, which is the stochastic switching between phases of growth and rapid shrinkage [7]. Polymerization phases terminate in catastrophes, where the MT switches to a state of rapid depolymerization. Depolymerization phases are terminated by rescue events, in which the MT switches back into a growing state. The dynamic instability is closely linked to the hydrolysis of tubulin dimers: MT catastrophe events are associated with the loss of the stabilizing GTP-cap through hydrolysis to GDP-tubulin within the MT.

The depolymerization rate of GDP-tubulin dimers is significantly higher than the depolymerization rate of GTP-dimers. However, catastrophes are more than phases of rapid depolymerization of the GDP-cap of a MT. This is strongly suggested by conformational changes and mechanical forces occurring during catastrophes: (i) in a MT catastrophe the protofilaments of MT fall apart and curl into characteristic 'ram's horn' conformations [8]; (ii) depolymerizing MTs can exert forces, which are important in mitosis if chromosomes are separated [1].

The curling into ram's horns is caused by a spontaneous curvature of GDP-tubulin dimers. This means hydrolysis gives rise to changes in the tubulin dimer conformation or the MT structure. Two different models have been discussed in the literature to describe the influence of hydrolysis on the mechanics of the MT, the allosteric model [9] and the lattice model [10, 11]. In the allosteric model, inter-dimer or intra-dimer bending angles change during hydrolysis [9, 12]. Hydrolysis of a tubulin dimer changes one or both of these angles [9]. If it is assumed that hydrolysis mainly changes the intra-dimer angle, this angle increases from 0° for straight GTP-dimers to 22° for

curved GDP-dimers [13]. In the lattice model, both states of the tubulin dimers are slightly bent and hydrolysis weakens the lateral interaction strength between dimers in neighboring protofilaments [9–11]. At present, the experimental evidence is not sufficient to rule out any of the two models. Also combinations of both models are possible, where hydrolysis affects both the intra-dimer angle (allosteric) and the interaction strength between laterally neighboring dimers (lattice).

The influence of tubulin dimer hydrolysis onto the mechanics of the MT lattice suggests that, vice versa, mechanical forces and torques acting on tubulin dimers or the MT structure also affect hydrolysis rates. This effect has not been considered in the literature before, and we will use the allosteric model with intra-dimer bending to study this coupling of hydrolysis and MT mechanics. Similar investigations should be done in the future for the lattice model.

Moreover, recent experiments also suggest that catastrophes are initiated in a multi-step process, which involves not a single rate-limiting event but a chain of at least two events, which are probably related to hydrolysis events [14]. Mechanical forces might be one possible way to orchestrate such a chain of hydrolysis events. Our results on the influence of MT mechanics on the hydrolysis pathway will give hints on the mechanism of catastrophe initiation.

There are numerous models for the growth dynamics of MTs, which either ignore catastrophe events and focus on the growing phase of MT dynamics [15–19], or which include catastrophes as explicit stochastic switching events on a macroscopic level following [20]. These approaches include details of the hydrolysis mechanism into the model for the catastrophe rate [21–24]. One focus of these approaches was the explanation of the behavior of MT growth dynamics under force.

In this paper, we want to concentrate on the coupling of hydrolysis events to MT mechanics. We will ignore the polymerization dynamics for simplicity and consider hydrolysis in MTs of fixed length without any external forces. In the end, we try to develop a microscopic model for the initiation of catastrophes based on hydrolysis events coupled to the mechanics of the MT lattice and additional rupture events within the MT lattice. This means that we will not include catastrophes as explicit stochastic events but obtain catastrophes as emerging events from hydrolysis coupled to mechanics within the MT. Our description will be microscopic on the level of tubulin dimers (i.e., not on the level of all-atom simulations as in [25, 27, 28]).

There exist already various models describing the stochastic dynamics of hydrolysis and the mechanics of MTs on the dimer level. They can be classified into different categories:

(i) There are purely ‘chemical’ models not taking into account the mechanics of the MT lattice but only including chemical rate constants for addition and removal of tubulin dimers and hydrolysis rates [21, 22, 29–35]. In these chemical models, phases of accelerated depolymerization can be observed if the cap mainly consists of GDP-tubulin. These phases of fast depolymerization are identified with catastrophe events. Different hydrolysis mechanisms such as random [30, 34], vectorial [18, 29], or mixed cooperative mechanisms [21, 22, 35, 36] are possible and have been discussed, but this issue is not settled for MT [32]. The model proposed by Flyvbjerg [21, 22] including both random and vectorial mechanisms in a cooperative mechanism has been successfully applied to fit catastrophe rates from the resulting first-passage statistics to zero GTP-cap length. The results suggest a strongly cooperative mechanism with mostly vectorial hydrolysis and a fairly small random component. However, if the results of [37] for the resulting GTP-cap length are used, the strong cooperativity leads to rather large GTP-caps as compared to experimental findings of up to three layers of GTP-tubulin [38–40]. In [35], on the other hand, a weakly cooperative mechanism with mostly random hydrolysis is found to describe experimental data on catastrophe rates best. In [40], a random hydrolysis mechanism has been successfully used to model typical MT length fluctuations on the nanometer scale. In [32], a coupled-random hydrolysis mechanism has been proposed, where the plus end GTP-dimer cannot hydrolyze but only dissociate. One advantage of many chemical models is that exact or, at least, approximative analytical results can be found [21, 22, 34–36], for example, for catastrophe frequencies, which can be easily compared to experimental data.

(ii) Chemical models also differ with respect to protofilament substructure. In some models the 13 protofilament substructure is ignored [18, 21, 22, 34, 35], more detailed models contain all 13 protofilaments explicitly [29–33]. Some of these more detailed ‘chemical’ models also include a possible influence of the neighboring protofilament state on hydrolysis [30, 31]. However, all of these models still deal with strictly rigid MTs.

(iii) Furthermore, there are purely ‘mechanical’ models on the level of single dimers, which include the possible bending of protofilaments and binding interaction between neighboring protofilaments [25, 27, 28, 41, 42], but do not model their influence onto chemical hydrolysis or polymerization rates.

(iv) Only the model proposed in [43] couples chemical and mechanical aspects of the MT lattice and considers the influence of mechanics on polymerization and depolymerization rates.

In all of these models, the interplay of mechanical forces and hydrolysis remains unaddressed so far. In this paper, we will add this aspect and focus on the influence of mechanical forces onto hydrolysis rates and its consequences for hydrolysis pathways and the initiation of catastrophe events.

2. Methods

2.1. Mechanical MT model

Each protofilament consists of $\alpha\beta$-tubulin heterodimers of length $d = 8$nm. MTs consist of 13 protofilaments forming a hollow tube of (outer) radius $R_o = 12.5$nm. GTP can bind to the β-tubulin and is hydrolyzed in the polymerized state.

In the following, we will employ the so-called allosteric model and assume that GTP-tubulin dimers are straight and assemble into straight protofilaments, whereas GDP-tubulin tends to form curved protofilaments with curvature radius 21 nm in the typical ram's horn configurations [13]. Protofilament curvature can be caused both by inter- and intra-dimer bending [9, 12]. If we assume that there is only intra-dimer bending during hydrolysis, a GDP-dimer acquires a bent configuration with an equilibrium angle of 22°. The tube formed by the 13 protofilaments is stabilized by lateral bonds between tubulin dimers in neighboring protofilaments. These bonds are assumed to be identical for GTP- and GDP-dimer within the allosteric model.

GTP-tubulin assembles into protofilaments (i.e., has a high polymerization rate and a low depolymerization rate), whereas GDP-tubulin tends to disassemble (i.e., has a depolymerization rate much higher than the polymerization rate) [39]. Within the MT protofilaments, GTP-tubulin is hydrolyzed into GDP-tubulin after a certain waiting time depending on the exact hydrolysis mechanism and hydrolysis rates. This gives rise to MTs consisting of an unhydrolyzed GTP-cap at the growing end and hydrolyzed GDP-tubulin behind this cap. Comparison of recent experimental measurements of MT length fluctuations on the nanometer scale and a random hydrolysis model suggests a cap size of ∼40 GTP-dimers corresponding to three layers of GDP-dimers [40, 43]. The structure of the cap will depend on the hydrolysis mechanism. For *random* hydrolysis, where dimers hydrolyze completely independent from each other [7, 43], the cap boundary is not sharp (in the sense that there are many GTP-/GDP-boundaries in the cap region) with an exponentially decaying GTP-tubulin concentration. For a *vectorial* mechanism, where hydrolysis propagates as a 'wave' because hydrolysis can only happen if the neighboring dimer is already in its hydrolyzed GDP-state [44], the cap boundary is sharp by definition. For *cooperative* models incorporating both mechanisms [21, 22, 36], we get a cap structure consisting of many GTP-islands with a characteristic dependence of the island size distribution and cap size on the cooperativity parameter [36, 37].

Because GTP-tubulin dimers are straight, they stabilize the MT as they do not stress lateral bonds between protofilaments. Intrinsically curved GDP-dimers, on the other hand, stress the lateral bonds and destabilize the MT lattice. In the following, we consider a MT with a fixed length, a stabilizing GTP-cap of fixed size and with a sharp cap boundary for simplicity (typically three layers of GTP-dimers). We formulate a mechanical model, which (i) incorporates dimer bending and lateral bonds between neighboring protofilaments, (ii) gives mechanically stable tubular structures in agreement with experimentally observe MT structures, and (iii) is as simple as possible.

MTs are hollow cylinders consisting of 13 protofilaments with outer radius $R_o = 12.5$ nm and inner radius $R_i = 8.5$ nm, where we assume each tubulin dimer to consist of two spherical tubulin monomers of size $d/2 = 4$ nm. Each protofilament is modeled by a chain of $M + 1$ $\alpha\beta$-tubulin dimers, which are longitudinally bound by intra-dimer and inter-dimer bonds. The total length of the MT is $L = (M + 1)d$ with the dimer length d. We only allow for intra-dimer bending at the $\alpha\beta$-junction within each dimer, see figure 1(a). The MT conformation is then described by bending angles of the $\alpha\beta$-dimer in the ith protofilament ($i = 1,...,13$) in the jth layer, where $j = M$ corresponds to the GTP-capped MT end and $j = 1$ to the GDP-end, see figure 1(b). We only allow for intra-dimer bending and regard the inter-dimer bonds as straight and fixed.

For the mathematical description, we can then group the β-tubulin in layer $j - 1$ with the α-tubulin in layer j into a straight 'rod' j oriented with angle $\theta_j^{(i)}$ in protofilament i. In the following we will describe the MT configuration in terms of these rods, as shown in figure 1(a). We fix $\theta_0^{(i)} = 0$ and parametrize the MT configuration by M angles $\theta_j^{(i)}$ $(j = 1,...,M)$ for each protofilament i. Vice versa, the bendable junction between rods $j - 1$ and j in protofilament i corresponds to the bendable $\alpha\beta$-junction of the dimer j with bending angle $\Delta\theta_j^{(i)} = \theta_j^{(i)} - \theta_{j-1}^{(i)}$. We note that the last β-tubulin monomer of the last tubulin dimer at the plus end in layer $j = M$ is not contained in any rod. Therefore, the hydrolysis state of the last tubulin dimers at the plus end of each protofilament will have no effect in our model, as further discussed below.

The minus end of every protofilament is fixed in the xy-plane. For simplicity, we do not take into account the helical pitch. We choose the MT axis as z-axis and define

$$\mathbf{v}_0^{(i)} = \begin{pmatrix} R\cos\phi^{(i)} \\ R\sin\phi^{(i)} \\ 0 \end{pmatrix} \tag{1}$$

as starting points of the first layer of rods. The polar angle of the ith protofilament is $\phi^{(i)} = i \cdot 2\pi/13$. Thus, the ending position $\mathbf{v}_j^{(i)}$ of the ith rod in the jth layer is given by

$$\mathbf{v}_j^{(i)} = \mathbf{v}_{j-1}^{(i)} + d\begin{pmatrix} \cos\phi^{(i)}\sin\theta_j^{(i)} \\ \sin\phi^{(i)}\sin\theta_j^{(i)} \\ \cos\theta_j^{(i)} \end{pmatrix}. \tag{2}$$

We assume that dimers or rods can only be displaced in radial direction, i.e., all polar angles $\phi_j^{(i)} = \phi^{(i)} = i \cdot 2\pi/13$ are fixed and independent of the layer number j. The azimuth angles $\theta_j^{(i)}$ of rods describe the radial displacements of dimers and are the configurational variables that are determined by mechanical energy minimization.

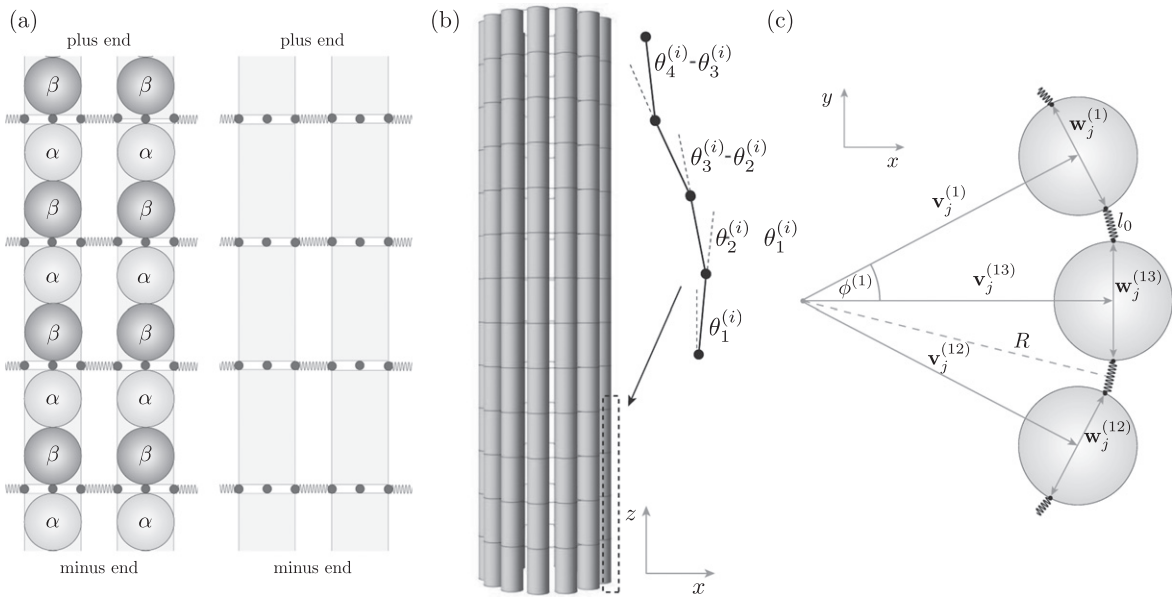

Figure 1. Schematic representation of the MT model. (a) Only the $\alpha\beta-$ junction of tubulin dimers can bend. Straight $\beta\alpha$-segments are grouped to stiff rods of length d and diameter $d/2$ for the mathematical description. Each rod has two interaction points for lateral bond springs at the surface of the rods at mid-height of the dimers, which means at the top end of the rods. (b) A specific configuration is characterized by the position angles $\theta_j^{(i)}$. Hydrolysis causes a shift of the preferred bending angle $\theta_{0,j}^{(i)}$ from 0° to 22° at the $\alpha\beta-$ junction. (c) Lateral bonds are modeled by spring interactions. The interaction points lie on the surface of the tubulin dimers.

We consider MT configurations that contain m_1 complete layers of hydrolyzed GDP-tubulin and $m_2 + 1$ complete layers of GTP-tubulin ($M + 1 = m_1 + m_2 + 1$); we focus on four layer GTP-caps with $m_2 = 3$. In accordance to the allosteric model we assume GTP-dimers to be straight with an equilibrium angle $\theta_0 = 0°$ and GDP-tubulin bent with an equilibrium angle $\theta_0 = 22°$. We consider deviations from these preferred equilibrium angles to be governed by an elastic bending energy with a characteristic bending rigidity κ. Therefore, we define the longitudinal bending energy stored in the MT lattice as

$$E_{\text{long}} = E_{\text{bend}} = \sum_{j=1}^{M} \sum_{i=1}^{13} \frac{\kappa}{2} \left(\theta_j^{(i)} - \theta_{j-1}^{(i)} - \theta_{0,j}^{(i)} \right)^2, \qquad (3)$$

with $\theta_0^{(i)} = 0$ fixed and the bending rigidity κ of individual tubulin dimers.

To obtain a tubular structure, we have to introduce lateral bonding. A reasonable and simple assumption is that only dimers in neighboring protofilaments interact laterally (reminiscent of some form of molecular bonds forming). Mechanical stability will require to introduce two contributions to these lateral interactions: one attractive binding contribution in form of a harmonic bond with a finite rest length and an additional hard-core-like repulsion, which basically prevents configurations with interpenetrating dimers.

For the attractive binding contribution, we assume that neighboring tubulin dimers interact via bonds between specific interaction points on the surface of the dimers. We use only one lateral bond per dimer, i.e., each dimer or each rod has two interaction points, which we locate on the surface at the top of each rod, see figure 1(a). We model tubulin dimers and rods with a spherical cross section of radius $d/4$ and assume that the bonds between neighboring dimers have a rest length l_0, see figure 1(c). We consider lateral stretching from the rest length l_0 to be harmonic with a characteristic spring constant k. The rest length l_0 can be determined by geometry; with the mean radius $R = \left(R_o + R_i\right)/2 = 10.5\text{nm}$ and assuming spherical tubulin monomers of radius $d/4$, we obtain

$$l_0 = 2\left(\sin \pi/13\right)\left[R - \left(d/4\right)\left(\cot \pi/13\right)\right] \simeq 1.14 \text{ nm}. \qquad (4)$$

If the equilibrium angle $\theta_{0,j}^{(i)}$ of a tubulin dimer changes from 0° to 22° by hydrolysis, this will strain the lateral bonds in the MT lattice. Because the interaction points for lateral bonds are located at the top of each rod (or at mid-height of each dimer, see figure 1(a)), hydrolysis of the last β-tubulin monomer of the last tubulin dimer at the plus end ($j = M$) does *not* strain the last bond. Therefore, the hydrolysis state of the tubulin dimers at the plus end of each protofilament at $j = M$ will have no effect on MT mechanics in our model. If we consider MT-configurations with GTP-caps consisting of $m_2 + 1$ complete layers of GTP-tubulin, only m_2 GTP-layers have an effect on MT mechanics. We therefore ignore the last layer of β-tubulin monomers at the plus end in the following, in particular in the MT hydrolysis patterns shown in figures 5–8 below. We point out that the last tubulin layer has a stabilizing effect also in our model as the stabilizing lateral bonds are contained in our model (at the top of the last rod, see figure 1(a)). However, this stabilizing effect is

Table 1. MT geometry parameters.

Dimer size d	8 nm
Monomer size $d/2$	4 nm
Outer radius R_o	12.5 nm
Inner radius R_i	8.5 nm
Mean radius R	10.5 nm
Spring length l_0	1.14 nm
Protofilament distance r	5.1 nm
Protofilament shift z_0	0.92 nm

independent of the hydrolysis state of the last layer and only depends on the hydrolysis states of the layers below. This point of view can be further justified because GTP-dimers at the plus end cannot hydrolyze as the last β-monomer has no inter-dimer contact [45].

In addition to the attractive lateral binding forces, we apply a strongly repulsive hard core interaction to avoid overlapping of tubulin dimers, which we model by a r^{-12} -potential. Accordingly, we define the total lateral mechanical energy by

$$\begin{aligned} E_{\mathrm{lat}} &= E_{\mathrm{spring}} + E_{\mathrm{hc}} \\ &= \sum_{j=1}^{M}\sum_{i=1}^{13}\frac{k}{2}\Big[\Big|\mathbf{v}_j^{(i)} - \mathbf{w}^{(i)} \\ &\qquad - \left(\mathbf{v}_j^{(i-1)} + \mathbf{w}^{(i-1)}\right)\Big| - l_0\Big]^2 \\ &\quad + \sum_{j=1}^{M}\sum_{i=1}^{13} k' \cdot \left(\left|\mathbf{v}_j^{(i)} - \mathbf{v}_j^{(i-1)}\right| - d/2\right)^{-12}, \end{aligned} \tag{5}$$

where $\pm\mathbf{w}^{(i)}$ are the vectors from the center of the spherical dimer cross section to the two interaction points on the dimer surface, k is the spring constant for the binding force and k' the strength of the repulsion.

As the stable configuration of a physical system is characterized by minimum free energy, we numerically calculate the minimum of the total energy functional

$$E = E_{\mathrm{long}} + E_{\mathrm{lat}} = E_{\mathrm{bend}} + E_{\mathrm{spring}} + E_{\mathrm{hc}} \tag{6}$$

with respect to the $13 \cdot (m_1 + m_2)$ variables $\theta_j^{(i)}$.

In the following, we often measure energies in units of the dimer bending rigidity κ. This shows that the dimensionless energy E/κ and, thus, our MT model is characterized by three remaining control parameters: the ratios k/κ and k'/κ control the MT mechanics; the ratio κ/k_BT of dimer bending rigidity and thermal energy controls the relevance of stochastic thermal fluctuations in comparison to mechanical forces. All relevant model parameters for MT geometry are summarized in table 1.

2.2. Model parameters for mechanically stable tubular structures

No direct experimental measurement of the microscopic mechanical parameters k and κ is available so far. However, there are a number of experiments determining the macroscopic elastic moduli of the MT lattice which could be related to the microscopic mechanical parameters. The lateral bond elasticity k can be deduced from measurements of the macroscopic shear modulus [25]. Moreover, molecular dynamics (MD) simulations of short MT protofilaments [25–28] can eventually give more direct information on the molecular scale parameters κ and k. The requirement to obtain a stable equilibrium MT structure, which is tubular and agrees with the experimentally observed geometry will put further constraints on the three parameters κ, k, and k' of our model.

The lateral bond elasticity k can be related to the macroscopic shear modulus G of the MT, which has been experimentally measured as $G \simeq 2\mathrm{pN/nm^2} = 2\mathrm{MPa}$ (at $T = 37°\mathrm{C}$) [46]. The two-dimensional shear modulus of the MT lattice is $G_{2D} = Gh$, where $h \simeq 4$ nm is the thickness of the MT lattice sheet, which is given by the size of a tubulin monomer. The shear energy per dimer is $e_{\mathrm{sh}} = hdrG\alpha^2/2$ with the distance $r = 2\pi R/13 \simeq 5.1$ nm between neighboring protofilament centers (where $R = \left(R_o + R_i\right)/2 = 10.5$ nm is the mean of outer and inner tube radius). In order to calculate the shear energy of the MT lattice properly, we have to take into account the helical pitch of 3/2 dimers per turn, which gives rise to a shift $z_0 \simeq 0.92$ nm between neighboring protofilaments. The rest length of lateral bond springs becomes $l_{0,\mathrm{hel}} = \left(l_0^2 + z_0^2\right)^{1/2} \simeq 1.46$ nm. Shearing of the MT lattice by a small angle α gives rise to elongation of the lateral springs from their rest length $l_{0,\mathrm{hel}}$ by $\Delta l = \Delta z z_0/l_{0,\mathrm{hel}}$, where $\Delta z = \alpha r$ is the relative displacement of protofilaments induced by shearing, see figure 2. Therefore, the shear energy per dimer can also be written as

$$e_{\mathrm{sh}} = \frac{1}{2}k\Delta l^2 = \frac{1}{2}k\frac{z_0^2 r^2}{l_{0,\mathrm{hel}}^2}\alpha^2.$$

Comparison with $e_{\mathrm{sh}} = hdrG\alpha^2/2$ gives an estimate

$$k = \frac{hdl_{0,\mathrm{hel}}^2}{z_0^2 r}G \simeq 7.69 k_BT\ \mathrm{nm}^{-2}. \tag{7}$$

In order to estimate the bending rigidity κ of single tubulin dimers, we can use existing MD simulation results on the distribution of protofilament curvatures. In [27], thermal fluctuations of the curvature radius of a protofilament consisting of three GTP- or GDP-tubulin dimers have been investigated by MD simulations and a distribution of protofilament curvature radii has been measured. A single protofilament with $N_p = 3$ coupled dimers will behave as a short semiflexible polymer of length $N_p d$. Each of the $N_p - 1$ $\alpha\beta$ -junctions with bending angle $\Delta\theta$ contributes a bending energy $e_{\mathrm{bend,j}} = \frac{1}{2}\kappa\Delta\theta^2 = \frac{1}{2}\kappa d^2 c_j^2$, where $c = \Delta\theta/d$ is the local curvature. The mean curvature $c_m = \frac{1}{N_p-1}\sum_{j=1}^{N_p-1} c_j$ of the

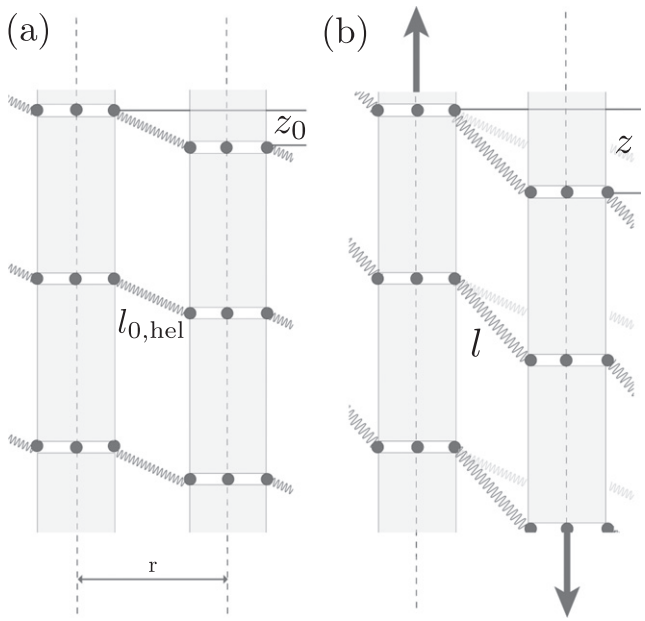

Figure 2. Deformation of lateral bond springs by shearing the MT lattice.

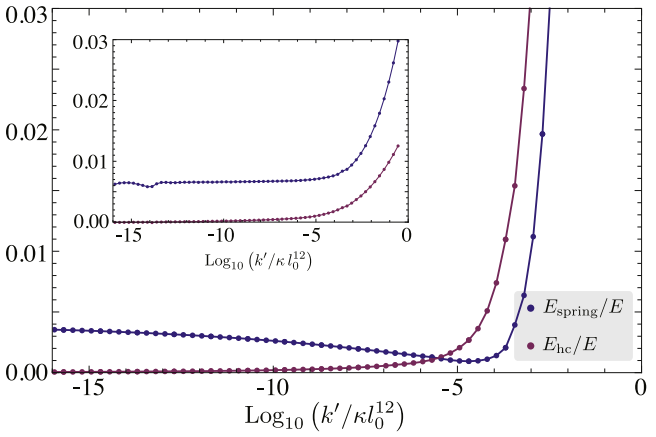

Figure 3. The fraction of hard-core energy E_{hc}/E of the total energy in comparison to the fraction of spring energy E_{hc}/E as a function of the dimensionless hard core parameter $\bar{k}' = k'/\kappa l_0^{12}$ for two different values $k/\kappa = 0.5\ \mathrm{nm}^{-2}$ and $k/\kappa = 0.005\ \mathrm{nm}^{-2}$ (inset) corresponding to strong and weak lateral bond springs.

protofilament exhibits Gaussian fluctuations with

$$\left\langle c_m^2 \right\rangle = \left\langle c_j^2 \right\rangle = \kappa d^2 / k_B T$$

and, thus, is distributed according to

$$p_c\left(c_m\right) \propto \exp\left(-\kappa d^2 c_m^2 / 2k_B T\right).$$

Then we can calculate the corresponding distribution of mean curvature radii $R = 1/c_m$,

$$p\left(R\right) = p_c\left(c_m\left(R\right)\right)\frac{1}{R^2} \propto \frac{1}{R^2}\exp\left(-\frac{d^2\kappa}{2k_B T}\frac{1}{R^2}\right), \qquad (8)$$

and find a maximum at $R_{\mathrm{max}}^2 = d^2\kappa/2k_B T$. In the MD simulations in [27] a most probable radius $R_{\mathrm{max}} \simeq 20\mathrm{nm}$ has been measured which leads to an estimate

$$\kappa = 2R_{\mathrm{max}}^2 k_B T/d^2 \simeq 12.5 k_B T \qquad (9)$$

for the dimer bending rigidity κ.

In [25, 27], the dimer bending rigidity κ was determined by applying equipartition to the mean square thermal fluctuations of bending angles as measured in the MD simulations of protofilaments containing three dimers. This approach gives much higher values $\kappa = 1.25 \times 10^4 \mathrm{pN\ nm} \sim 3000 k_B T$ [25] and $\kappa \sim 300 - 400 k_B T$ [27], which differ from each other and our above estimate (9). Currently we have no explanation for these discrepancies.

We also have to fix the value of the hard core parameter k'. Because the hard core repulsion only serves as auxiliary interaction in order to avoid an unphysical overlapping of neighboring dimers, we want to use values for k' which do not influence the MT equilibrium configuration appreciably. Therefore, we want to choose k' such that the hard core interaction energy E_{hc} remains much smaller than the the bending energy E_{bend} and the spring energy E_{spring}. In figure 3, we show the relative contributions of both energies to the total energy. For values $k'/\kappa l_0^{12} < 10^{-5}$ the hard core interaction has negligible influence on the MT equilibrium configuration. We therefore use $k'/\kappa = 10^{-6}\ \mathrm{nm}^{12}$ in the following.

Finally, the value of k/κ is constrained by the requirement that the equilibrium MT forms a tubular structure. We find that for weak lateral springs, i.e., too small values of k/κ the stabilizing effect of a GTP-cap is lost and MTs spontaneously acquire a strongly bent shape similar to the ram's horn configuration of depolymerizing catastrophic MTs. We studied this effect systematically by calculating MT configurations of minimal mechanical energy for k/κ in the range $k/\kappa = 10^{-5}\ \mathrm{nm}^{-2} \ldots 1\ \mathrm{nm}^{-2}$, see figure 4. Because such forms have not been observed experimentally, we conclude that a reasonable lower bound for k/κ is

$$k/\kappa \geqslant 0.001\ \mathrm{nm}^{-2}. \qquad (10)$$

Note that with our above estimates (7) for k and (9) for κ we find $k/\kappa \simeq 0.61\ \mathrm{nm}^{-2}$, which is far above this bound. The much larger values of κ that have been obtained in [25, 27] as discussed above would lead to a ratio k/κ close to the lower bound (10).

Because of the considerable uncertainty in the estimates for k and κ, we will investigate values $k/\kappa = 0.005\ \mathrm{nm}^{-2}$ close to the lower bound as an example for weak lateral springs and $k/\kappa = 0.5\ \mathrm{nm}^{-2}$ as an example for strong lateral springs in the following.

2.3. Discussion of alternative models

In this section, we want to discuss alternative models. In a conceptually simpler model we could put single interaction points for the lateral bond springs at the centers of the tubulin dimers. We investigated such simpler models and found that equilibrium configurations exhibit 'wrinkled' tubes (wrinkles

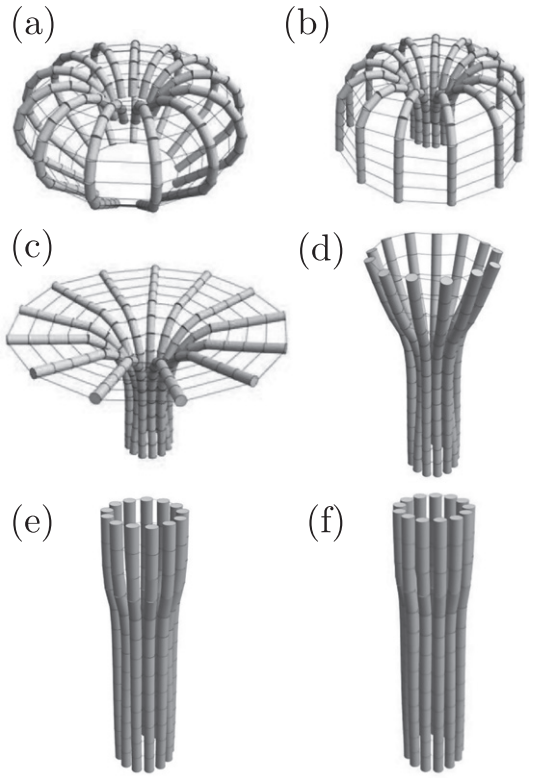

Figure 4. Mechanical equilibrium configuration of MTs for $k/\kappa =$ (a) 10^{-5}, (b) 1.8×10^{-4}, (c) 2×10^{-4}, (d) 10^{-3}, (e) 10^{-2}, and (e) 10^{-1} nm^{-2} ($k'/\kappa = 10^{-6}$ nm^{12}). MTs are stabilized by a three layer GTP-cap $(m_1 = 10, m_2 = 3)$.

forming along the protofilament axis) for sufficiently long MTs. Wrinkling can not be prevented by additional hard core repulsion terms. Therefore, such models do not agree with the experimental observations of tubular MTs.

Our model resembles other mechanical models proposed in [41, 43, 47]. The mechanical model proposed by Molodtsov *et al* [41, 47] also contains a bending energy and lateral bonds, which are modeled as harmonic springs around their equilibrium length. In [41, 47], four interaction points and two lateral springs are introduced per dimer and the helical structure is taken into account in contrast to our model. Moreover, only inter-dimer bending is considered. Molodtsov *et al* use much larger values $k \sim 150 k_B T$ nm^{-2} than our estimate $k \simeq 7.69 k_B T$ nm^{-2}, see (7). Their value is obtained from an estimate of the activation energy for bond rupture, assuming a certain one-parameter form of the lateral bond potential, which tightly couples the parameter for bond elasticity to the bond rupture forces. We rather used values for the bond elasticity confirming with the macroscopic shear modulus of a protofilament sheet following [25] and consider the bond rupture force as an *independent* parameter (see section 3.2 below). Molodtsov *et al* then also estimate much higher values of κ by applying a similar constraint for k/κ as we obtained above (10), violation of which gives rise to strongly outward bending cap configurations even in the presence of a GTP-cap. In contrast, we tried to obtain an estimate for κ from microscopic MD simulation data.

The mechanical model proposed by Van Buren *et al* [30, 43] also contains a bending energy and lateral bonds, which are modeled as harmonic springs of zero rest length. In addition, the model also includes longitudinal harmonic bond springs to model protofilament stretching and torsion elasticity, i.e., an elastic energy for the angles $\phi_j^{(i)}$, which are fixed to $\phi_j^{(i)} = \phi^{(i)} = 2\pi i \big/ 13$ in our model.

Finally, we want to point out that the MT bending rigidity κ_{MT} and, thus, its persistence length, is not directly related to the dimer bending rigidity κ in mechanical models. It is mainly related to the stiffness of longitudinal bonds between neighboring dimers on the same protofilament, which are stretched and compressed in bending deformations of the tube. Longitudinal bond stiffnesses are absent in our model as we do not consider shape fluctuations of the whole tube but are included in the models used in [41, 43, 47] and have also been discussed in [48]. Longitudinal bonds are found to be much stiffer than lateral bonds. In [48] it has been shown that the MT persistence length becomes length dependent as it contains both bending contributions related to longitudinal bonds and shear contributions related to the lateral bonds. We do not expect the longitudinal bond stiffness, the lateral bond stiffness k or the dimer bending rigidity κ themselves to be length dependent.

2.4. Coupling of hydrolysis and MT mechanics

In the allosteric model, hydrolysis of GTP-tubulin dimers to GDP-tubulin dimers within the MT leads to bending of the dimer, i.e., a change in the equilibrium dimer angle θ_0. This results in mechanical forces and torques in the MT lattice, which are transmitted by the harmonic binding forces between protofilaments and which drive the MT lattice to a new equilibrium state.

We can view θ_0 as the reaction coordinate of hydrolysis such that, in the absence of mechanical forces, hydrolysis of single dimers is characterized by a free energy profile $F_h(\theta_0)$ with a free energy minimum corresponding to a GTP-dimer at $\theta_0 = 0°$ and a second minimum corresponding to the GDP-dimer state at $\theta_0 = 22°$. Because of the free energy $\Delta G_{\mathrm{GTP}} \simeq 5 k_B T$ released by hydrolysis of GTP within the MT lattice [39], the second minimum is lower by at most $F_h(0°) - F_h(22°) < \Delta G_{\mathrm{GTP}} \simeq 5 k_B T$.

Because GTP hydrolysis can generate mechanical forces within the MT, mechanical forces also influence the hydrolysis rate of GTP-dimers. This influence can be quantified using Bell theory [49]. For each equilibrium angle $\theta_0 \equiv \theta_{0,j}^{(i)}$ of a given dimer we can also calculate the mechanical total equilibrium energy $E(\theta_0)$ of the MT lattice. The relevant free energy profile for hydrolysis, that takes into account the mechanics of the surrounding MT lattice, is $F_h(\theta_0) + E(\theta_0)$. Using θ_0 as a reaction coordinate there will be a rate limiting free energy barrier ΔF_h for an intermediate $0° < \theta_{0,\max} < 22°$. The height and the exact angle $\theta_{0,\max}$ of this energy barrier will

also be modified by the corresponding mechanical contribution to $\Delta F_h + \Delta E$. If we neglect a possible shift of the barrier angle, we have $\Delta E = E\left(\theta_{0,\max}\right) - E\left(0^\circ\right)$. We have currently no information on the detailed free energy profile $F_h\left(\theta_0\right)$ of the hydrolysis reaction; we only have information on the hydrolysis rates themselves, which should be related to the barrier height ΔF_h via the Arrhenius law. To proceed, we simply assume $\theta_{0,\max} = 11^\circ$ in the following. One important point regarding the influence of the mechanics of the MT lattice onto the hydrolysis rates is the following: *differences* between hydrolysis rates at different sites in the MT lattice are not governed by ΔF_h, which is identical for all MT lattices sites, but rather by the mechanical contribution ΔE to the barrier, which we want to estimate now.

We know that the total mechanical energy is a quadratic function of θ_0 via the bending energy contribution in (3). In order to determine ΔE for hydrolysis we have to increase θ_0 from 0° to $\theta_{0,\max}$ to obtain the saddle point value ΔE. Because we assume that a single hydrolysis reaction is faster than mechanical relaxation of the MT lattice, we increase θ_0 for *fixed* values of the configuration angles $\theta_j^{(i)}$. We assume an approximately linear dependence

$$E\left(\theta_0\right) - E\left(0^\circ\right) \approx \left(E\left(\delta\right) - E\left(0^\circ\right)\right)\theta_0/\delta$$

for a small angle δ, and estimate ΔE numerically using $\delta = 1^\circ$ and assuming $\theta_{0,\max} = 11^\circ$ for the position of the barrier. This results in the estimate

$$\Delta E = E\left(11^\circ\right) - E\left(0^\circ\right) \simeq 11\left(E\left(1^\circ\right) - E\left(0^\circ\right)\right) \qquad (11)$$

(calculated for fixed values of all configuration angles $\theta_j^{(i)}$). According to its definition, ΔE will be small (eventually even negative) for hydrolysis of a given dimer if there are mechanical forces in the MT lattice that pull the dimer into its bent GDP-configuration.

This mechanical shift of the free energy barrier for the hydrolysis reaction will modulate the hydrolysis rate r_h of a dimer according to

$$r_h\left(\Delta E\right) = r_h\left(0\right)\exp\left(-\Delta E/k_BT\right) \qquad (12)$$

following Bell [49]. In particular, this leads to *site-dependent* hydrolysis rates, which depend on the position of the dimer in the MT lattice via the mechanical forces acting on it at that position. We conclude that the interaction via the mechanics of the MT lattice can give rise to possible correlation effects in the hydrolysis dynamics, which have not been taken into account before.

Our simulation algorithm for the most probable hydrolysis pathway (see section 3.1 below) will be based on two assumptions regarding the time scales for hydrolysis and mechanical relaxation: (i) a single hydrolysis reaction is fast compared to mechanical relaxation, which was the basis for calculating the modulated hydrolysis rate (12), and (ii) mechanical relaxation is faster than the time *between* successive hydrolysis events (set by the hydrolysis rate r_h^{-1}) such that we relax the MT lattice mechanically between successive hydrolysis events.

2.5. Hydrolysis and mechanical model parameters

Within the MT GTP-dimers are hydrolyzed into GDP-dimers. The backward reaction is not observed. This puts a constraint on the mechanical model parameters because it implies that the total mechanical energy difference during hydrolysis of a certain dimer, $\Delta E_h = E\left(22^\circ\right) - E\left(0^\circ\right)$, has to be much smaller than the chemical energy $\Delta G_{\mathrm{GTP}} \simeq 5k_BT$ released by GTP hydrolysis in the absence of any mechanical forces [39], $\Delta E_h \ll \Delta G_{\mathrm{GTP}}$.

We consider the situation where the MT is still stabilized by the GTP-cap to a tubular configuration such that all angles $\theta_j^{(i)}$ are small. Then, hydrolysis of a single dimer (in layer j and protofilament i) increases its rest angle and strains the surrounding MT lattice. If the lateral interaction springs are sufficiently strong to stabilize a tubular MT configuration, the change $\Delta E_{\mathrm{spring}}$ in the lateral spring energies by this hydrolysis can be neglected as compared to the change ΔE_{bend} in bending energy such that the total mechanical energy increase during hydrolysis is approximated by

$$\begin{aligned}\Delta E_h \approx \Delta E_{\mathrm{bend}} &= \frac{\kappa}{2}\left(\theta_j^{(i)} - \theta_{j-1}^{(i)} - 22^\circ\right)^2 \\ &\quad - \frac{\kappa}{2}\left(\theta_j^{(i)} - \theta_{j-1}^{(i)}\right)^2 \\ &\approx \frac{\kappa}{2}\left(22^\circ\right)^2. \end{aligned} \qquad (13)$$

Then, the condition $\Delta E_h \ll \Delta G_{\mathrm{GTP}} \simeq 5k_BT$ implies an upper bound on the dimer bending rigidity κ,

$$\kappa \ll 2\Delta G_{\mathrm{GTP}}\frac{1}{\left(22^\circ\right)^2} \simeq 68k_BT\ \mathrm{rad}^{-2}. \qquad (14)$$

Our above estimate (9), $\kappa \simeq 12.5k_BT$, from analyzing MD simulation results for protofilament curvature radii distributions obeys the constraint (14). The other estimates $\kappa \sim 3000k_BT$ from [25] and $\kappa \sim 300k_BT$ from [27], however, violate this constraint. If κ-values violating the upper bound (14) are confirmed experimentally in the future, this can be a hint that the allosteric model itself, i.e., the assumption that GTP hydrolysis changes the tubulin dimer angle, is inconsistent.

Within the allowed upper bound $\Delta E_h \leqslant \Delta G_{\mathrm{GTP}}$, we can distinguish two limits for the hydrolysis rates: (i) if $\Delta E \ll k_BT$, the influence of the mechanical shift ΔE of the free energy barrier for the hydrolysis reaction is small, and we expect purely 'chemical' models as defined in the introduction to be essentially correct. (ii) If $\Delta E \gg k_BT$, on the other hand, the mechanical shift ΔE dominates the hydrolysis rates according to (12) and we expect a strong interplay between MT mechanics and hydrolysis.

In limit (ii), the dimer to be hydrolyzed next is mainly determined by the mechanical shifts ΔE of the free energy barrier for the hydrolysis reaction; the GTP-dimer with the

smallest ΔE will be hydrolyzed next, eventually under additional restrictions depending on whether we consider a vectorial or random hydrolysis mechanism. Only if several GTP-dimers have a similar ΔE, the next hydrolysis event will be stochastic among these dimers. Therefore, the order of hydrolysis of GTP-dimers within the MT lattice (the hydrolysis pathway) is mainly determined by the hydrolysis mechanism (vectorial or random) *and* the mechanical energies ΔE and exhibits much less stochasticity as compared to limit (i), as discussed below in the results section.

We will now explore under which condition we can expect such mechanically dominated hydrolysis order, i.e., under which conditions $\Delta E \geqslant k_B T$ holds. The mechanical shift ΔE of the energy barrier for the hydrolysis reaction should be smaller than total mechanical energy change ΔE_h during hydrolysis, $\Delta E \leqslant \Delta E_h$ resulting in a condition $\Delta E_h \geqslant \Delta E \geqslant k_B T$ or (using (13))

$$\kappa \geqslant 2k_B T \frac{1}{\left(22^\circ\right)^2} \simeq 14 k_B T \text{ rad}^{-2}. \tag{15}$$

For smaller values of κ, we expect to find hydrolysis rates, which are essentially independent of mechanical forces developing in the MT lattice.

Our above estimate (9), $\kappa \simeq 12.5 k_B T$, from analyzing MD simulation results for protofilament curvature radii distributions violates condition (15) only weakly. The other estimates for κ from [25, 27], however, give much higher values of κ supporting mechanically dominated hydrolysis rates.

3. Results

We use the mechanical model introduced above to investigate how mechanical forces influence and direct hydrolysis pathways and how catastrophe events emerge if lateral bond rupture is included.

3.1. Hydrolysis pathways

We explore results for a mechanically dominated hydrolysis rate where the mechanical shift of the free energy barrier for the hydrolysis reaction is much larger than the thermal energy $1k_B T$. Therefore, our results will apply if both bounds (14) and (15) are met, i.e., in a range $14k_B T \leqslant \kappa \ll 68 k_B T$ of dimer bending rigidities. This regime is conceptually interesting because correlation effects in the hydrolysis dynamics introduced via the mechanics of the MT lattice become maximal. Moreover, this parameter range for the tubulin dimer bending rigidity κ cannot be ruled out at present because different estimates for κ are deviating and not reliable. Our above estimate $\kappa \simeq 12.5 k_B T$, see (9), is close to the lower boundary of the considered κ-range.

If hydrolysis is mechanically dominated ($\Delta E \gg k_B T$), the hydrolysis pathways, i.e., the order of hydrolysis of dimers within the MT, is mainly determined by the mechanical shift ΔE of the energy barrier for the hydrolysis reaction: the dimer to be hydrolyzed next with highest probability is the GTP-dimer with the smallest ΔE among all GTP-dimers accessible by the hydrolysis mechanism. For random hydrolysis all GTP-dimers are accessible, for vectorial hydrolysis only the GTP-dimers at the cap boundary. Because the dimensionless energies $\Delta E/\kappa$ only depend on the parameter k/κ, the hydrolysis pathway is entirely determined by this mechanical parameter for both mechanisms. As a result of mechanically dominated hydrolysis, the choice of a certain hydrolysis pathway becomes much less stochastic: from the large number of chemically possible pathways only relatively few have considerable statistical weight if the influence of mechanics is dominant for $\Delta E \gg k_B T$. Therefore, the concept of a *most probable hydrolysis pathway*, which is the hydrolysis pathway with the highest statistical weight, is reasonable in this limit.

In the simulation, we determine the most probable hydrolysis pathway by the following algorithm: we relax the mechanical forces in the MT lattice by energy minimization for a given hydrolysis state. Next, we calculate the mechanical energy shifts ΔE for each GTP-dimer which can be hydrolyzed according to the assumed hydrolysis mechanism (random or vectorial). We calculate ΔE according to (11). Then, out of these GTP-dimers, we choose the one with the minimal ΔE and, thus, the highest hydrolysis rate according to (12) to be hydrolyzed next. Then, we relax the MT lattice again mechanically, and so on.

The condition $\Delta E \gg k_B T$ is necessary but not sufficient to select a hydrolysis pathway uniquely, i.e., render the hydrolysis deterministic: if several GTP-dimers have a similar ΔE, the next hydrolysis event will be essentially stochastic among these dimers. The hydrolysis pathway becomes deterministic only if also *differences* $\Delta\Delta E$ between the ΔE for different GTP-dimers within the MT are much larger than the thermal energy, i.e., $\Delta\Delta E \gg k_B T$.

As discussed in the introduction, the correct hydrolysis mechanism is not exactly known. Therefore we consider both vectorial and random hydrolysis separately in the following. We address the question how the mechanical forces direct the hydrolysis pathway for both mechanisms and as a function of the parameter k/κ. We will consider two exemplary values: $k/\kappa = 0.005\ \text{nm}^{-2}$ close to the lower bound (10) as an example for weak lateral springs and $k/\kappa = 0.5\ \text{nm}^{-2}$ as an example for strong lateral springs in the following.

In order to isolate effects of MT mechanics onto the hydrolysis pathway, we ignore the polymerization dynamics and consider hydrolysis in MTs of fixed length with a stabilizing GTP-cap consisting of three layers ($m_1 = 20$ and $m_2 = 3$).

3.1.1. Random hydrolysis. For random hydrolysis the chemical hydrolysis rate $r_h(0)$ of a given GTP-dimer is independent of the hydrolysis state of its neighbors, see (12). Therefore, all GTP-dimers in the cap can be hydrolyzed with equal probability if mechanics is neglected.

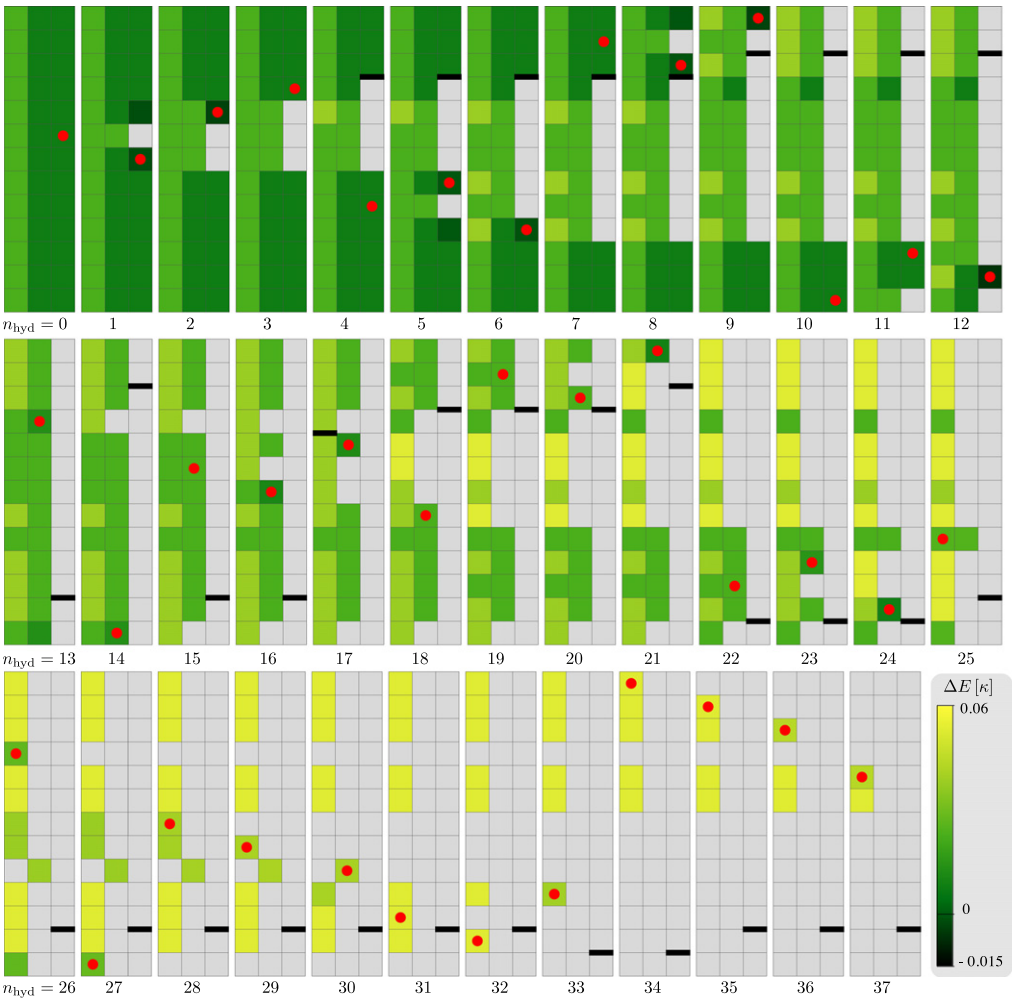

Figure 5. Random hydrolysis: most probable hydrolysis pathway of a MT with a three layer GTP-cap with strong lateral bond springs $\left(k/\kappa = 0.5\ \mathrm{nm}^{-2}\right)$. Each 13×3 rectangle in the sequence of 38 hydrolysis steps shows the hydrolysis state of the three layer GTP-cap (MT plus end on the right side): squares symbolize dimers; grey squares represent hydrolyzed GDP-dimers; green squares represent GTP-dimers color-coded for their respective $\Delta E/\kappa$. The red dot marks the dimer to be hydrolyzed next. The thick black vertical line marks the lateral bond under maximal force, see figure 9(a).

For random hydrolysis in the absence of mechanical forces, all GTP-dimers in the cap are accessible for hydrolysis with equal probability, and in a MT with a GTP-cap size of three layers ($m_2 = 3$) there are 39! equally probable hydrolysis pathways. For mechanically dominated random hydrolysis, on the other hand, it is always the dimer with smallest ΔE among all GTP-dimers, which is hydrolyzed next with the highest probability. As a result there emerges a *most probable hydrolysis pathway*, which is shown in figures 5 and 6 for a MT with $m_1 = 20$ and $m_2 = 3$ and strong springs ($k/\kappa = 0.5\ \mathrm{nm}^{-2}$, figure 5) or weak springs ($k/\kappa = 0.005\ \mathrm{nm}^{-2}$, figure 6). These figures show the sequence of 38 hydrolysis states of the 3x13 dimer cap (from $n_{\mathrm{hyd}} = 0$ GDP-dimers to $n_{\mathrm{hyd}} = 37$ GDP-dimers). GTP-dimers are represented by green squares, hydrolyzed GTP-dimers by grey squares.

If there are several GTP-dimers with similarly small ΔE, such that $\Delta\Delta E \leqslant k_B T$, they can be hydrolyzed with comparable probability, and there are other hydrolysis pathways which are similarly probable. The values of ΔE of different GTP-dimers (measured in units of κ) are indicated in the most probable hydrolysis pathways in 5 and 6 by color-coding. The existence of a unique, dark green square in a cap indicates the existence of a unique next hydrolysis spot, which is separated by a large $\Delta\Delta E$ from other possible hydrolysis spots. Small color differences indicate small values of $\Delta\Delta E$, such that the next hydrolysis spot should be chosen essentially stochastic among the dimers with darkest green colors. Then there exist other pathways competing to the ones shown in 5 and 6, which occur with comparable probability.

For random hydrolysis, figures 5 and 6 show that the most probable hydrolysis pathways are very similar for strong and weak lateral bond springs. Two features of the influence of mechanics can be deduced from figures 5 and 6:

(i) Hydrolysis is favored in the front layer of the GTP-cap towards the plus end (see states $n_{\mathrm{hyd}} = 1, 14, 27$). In the front layer, the mechanical strain from the bending of the GDP-dimers behind the cap gives rise to the strongest

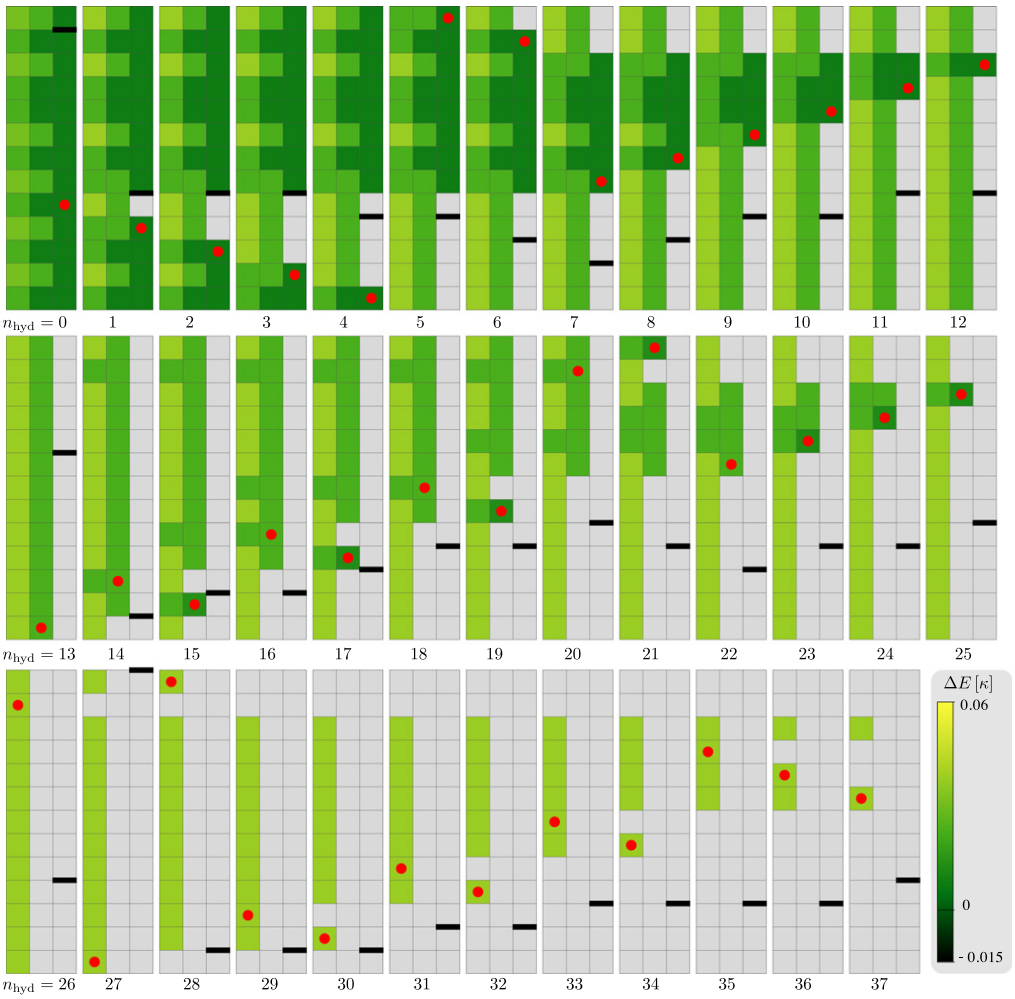

Figure 6. Random hydrolysis: most probable hydrolysis pathway of a MT with a three layer GTP-cap with weak lateral bond springs ($k/\kappa = 0.005\ \mathrm{nm}^{-2}$). Representation as in figure 5. The thick black vertical line marks the lateral bond under maximal force, see figure 9(b).

outward bending moments on a dimer via outward pulling forces exerted by the lateral springs.

(ii) After hydrolysis has started in a layer, there is a strong preference that this layer becomes completely hydrolyzed before it proceeds in the next layer. Together with point (i) this gives rise to a very regular hydrolysis pathway if mechanics is taken into account, although the underlying chemical hydrolysis rule is random.

(iii) There is a strong preference for GTP-dimers with two lateral GDP-neighbors to be hydrolyzed (see, for example, states $n_{hyd} = 12, 17, 20, 21$ in figure 5). These isolated straight GTP-dimers are pulled outward by already hydrolyzed and, thus, bent GDP-neighbors.

3.1.2. Vectorial hydrolysis. For vectorial hydrolysis, only dimers whose longitudinal neighbor (towards the minus end) is already hydrolyzed into GDP-tubulin are accessible for hydrolysis. Then there is a sharp interface between GDP- and GTP-dimers, which propagates towards the plus end. For mechanically dominated vectorial hydrolysis, the GTP-dimer with the smallest ΔE among all GTP-dimers at the GTP-GDP interface is hydrolyzed next.

Again, for mechanically dominated vectorial hydrolysis, there is a most probable hydrolysis pathway, which is shown in figures 7 and 8 for a MT with $m_1 = 20$ and $m_2 = 3$ and strong springs ($k/\kappa = 0.5\ \mathrm{nm}^{-2}$, figure 7) or weak springs ($k/\kappa = 0.005\ \mathrm{nm}^{-2}$, figure 8) in terms of the sequence of 38 hydrolysis states of the 3x13 dimer cap. For vectorial hydrolysis, there are also GTP-dimers which cannot be hydrolyzed because they are not at the GTP-GDP interface, i.e., there is no hydrolyzed neighboring GDP-dimer towards the minus end. These dimers are shown in white color. Only hydrolyzable GTP-dimers at the GTP-GDP interface are represented by green squares, hydrolyzed GTP-dimers by grey squares as before.

We recognize marked differences as compared to the random hydrolysis:

(i) Because of the vectorial constraint, hydrolysis has to start in the back layer of the GTP-cap towards the minus end, where the GTP-GDP interface is located. It cannot advance directly to the front layer as for random hydrolysis.

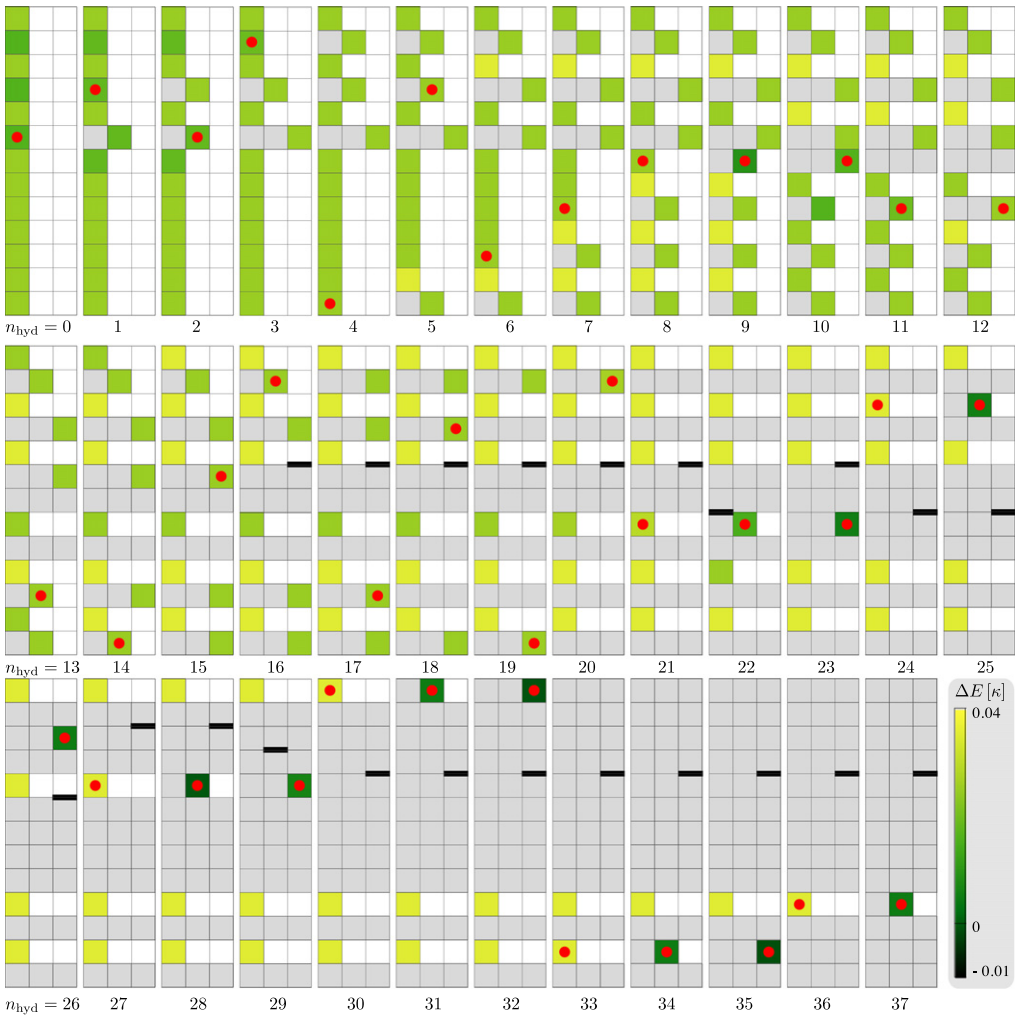

Figure 7. Vectorial hydrolysis: most probable hydrolysis pathway of a MT with a three layer GTP-cap with strong lateral bond springs $\left(k/\kappa = 0.5\ \mathrm{nm}^{-2}\right)$. Each 13×3 rectangle in the sequence of 38 hydrolysis steps shows the hydrolysis state of the three layer GTP-cap (MT plus end on the right side): squares symbolize dimers; grey squares represent hydrolyzed GDP-dimers; green squares represent GTP-dimers at the boundary of the GTP-cap, color-coded for their respective $\Delta E/\kappa$. White squares represent GTP-dimers, which are not at the cap boundary and, thus, cannot be hydrolyzed in a vectorial mechanism. The red dot marks the dimer to be hydrolyzed next. The thick black vertical line marks the lateral bond under maximal force, see figure 10(a).

(ii) There is a strong tendency to continue hydrolysis on the same protofilament (see states $n_{\mathrm{hyd}} = 1, 2, 3$ or $n_{\mathrm{hyd}} = 9, 10, 11$ in figure 7). If the hydrolysis front has advanced to the next layer on one protofilament, the bending forces from the hydrolyzed dimers behind the front give rise to a strong outward bending moment on the next GTP-dimer, which favors its hydrolysis. This force is transmitted via the lateral bonds to neighboring protofilaments in the MT lattice.

(iii) As for random hydrolysis, there is a preference for GTP-dimers with one or two lateral GDP-neighbors to be hydrolyzed (see, for example, states $n_{\mathrm{hyd}} = 10, 22, 23, 25, 26$ in figure 7).

(iv) The effects (ii) and (iii) combine to a 'nucleation-like' behavior: once a nucleus of three neighboring hydrolyzed GDP-dimers has formed in a layer, the hydrolysis front tends to advance up to the plus end on one of the protofilaments (states $n_{\mathrm{hyd}} = 3, 4, 5$ in figure 8). This effect is more pronounced for weak lateral bond springs.

In the next section we will see that the first advance of the hydrolysis front to the plus end is typically linked to a pronounced increase of the lateral bond forces, in particular for weak lateral bonds. If lateral bonds are allowed to rupture, this increase in forces can initiate catastrophe events. The last feature (iv) of a nucleus of three GDP-dimers that has to assemble before the hydrolysis front will reach the plus end could be an explanation of the experimental finding of two rate-limiting steps, which are involved in the initiation of a catastrophe [14].

3.2. Lateral bond rupture and catastrophes

During a catastrophe, it is experimentally observed that the protofilaments of a MT fall apart and curl into 'ram's horn'

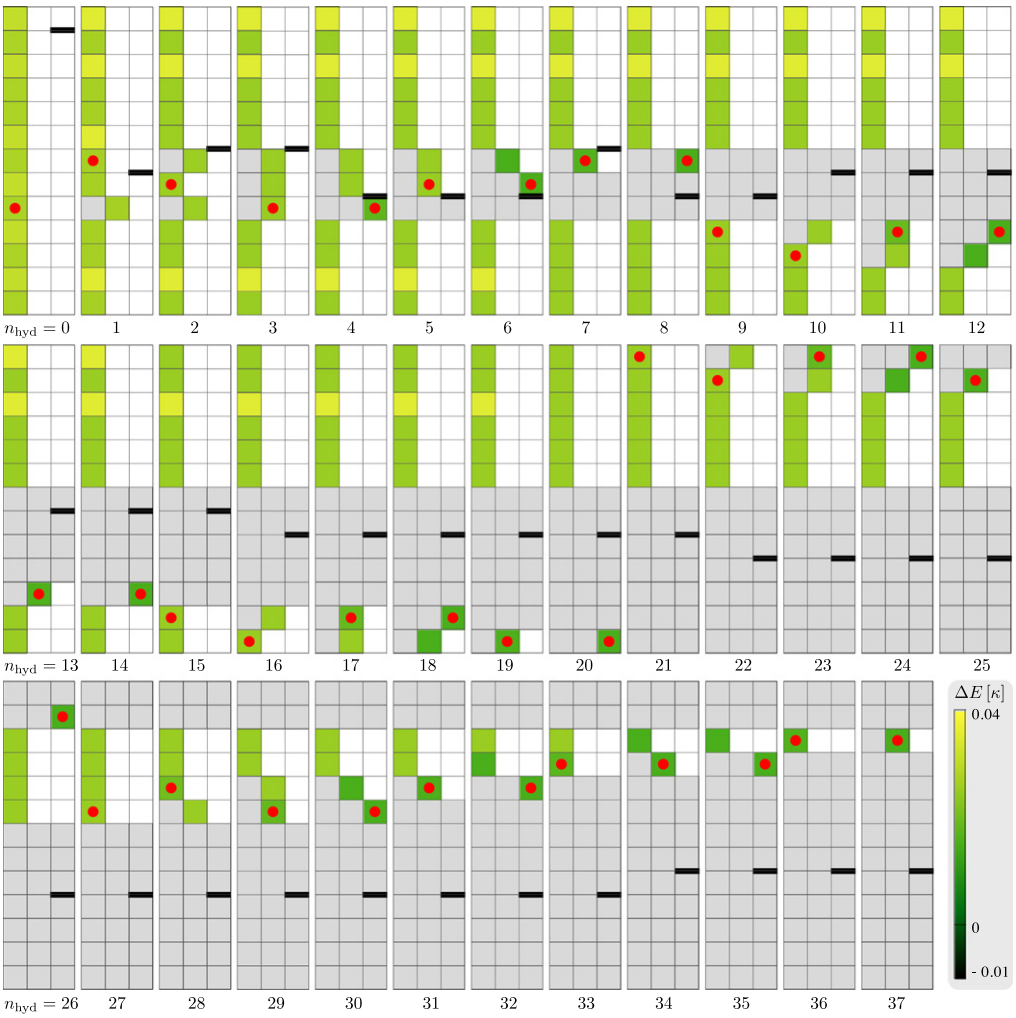

Figure 8. Vectorial hydrolysis: most probable hydrolysis pathway of a MT with a three layer GTP-cap with weak lateral bond springs ($k/\kappa = 0.005\ \mathrm{nm}^{-2}$). Representation as in figure 7. The thick black vertical line marks the lateral bond under maximal force, see figure 10(b).

conformations as a result of the 22° equilibrium angle of hydrolyzed GDP-dimers. This implies that protofilaments separate during catastrophes, i.e., lateral bonds between dimers in neighboring protofilaments will rupture.

Bond rupture is an activated process, and the bond rupture rate under force, $r_{\mathrm{rup}}\left(F\right) = r_{\mathrm{rup}}\left(0\right)\exp\left(F/F_{\mathrm{rup}}\right)$, increases exponentially above a characteristic rupture force F_{rup} according to Bell theory [49]. In a simplified approach, we can ignore stochastic rupture effects and assume that all lateral bonds under forces $F > F_{\mathrm{rup}}$ rupture. One problem is that there is currently no microscopic information on values for the rupture force F_{rup}. In [47], an activation energy for the rupture process was estimated from the depolymerizing velocity of catastrophic MTs as $E_{\mathrm{rup}} \simeq 10 k_B T$. Together with a characteristic bond length of $\simeq 0.25$nm used in [47], one arrives at very large rupture forces $F_{\mathrm{rup}} \sim 160$pN.

3.2.1. Maximal lateral bond force. Here we want to take a different approach and ask, which rupture forces can initiate catastrophe-like events within our mechanical model of the MT. To answer this question we consider the most probable hydrolysis pathway and calculate the maximal lateral bond force F_{max} within the MT lattice at every hydrolysis step. The results are shown in figure 9 for random hydrolysis and figure 10 for vectorial hydrolysis. The location of the lateral bond under maximal force within the GTP-cap is shown in the corresponding figures 5–8 as thick black line.

For random hydrolysis, mechanical forces favor hydrolysis at the last layer of the GTP-cap towards the plus end. For random hydrolysis and strong lateral bonds, see figure 9(a), we see a strong increase in the maximal bond force F_{max} after hydrolysis of $n_{\mathrm{hyd}} = 14$ dimers. At this point, the first dimer in the second to last layer is hydrolyzed after complete hydrolysis of the last layer at the plus end. For weak lateral bonds, see figure 9(b), we even see a periodic layer-by-layer pattern in the increase of F_{max} with pronounced jumps at $n_{\mathrm{hyd}} = 1, 14, 27$, where hydrolysis reaches the next layer starting from the plus end. In the corresponding figures 5 for strong lateral bonds and 6 for weak lateral bonds, the location of the maximally strained lateral bond is shown as thick black line. The maximally strained bond is at the plus end layer of the GTP-cap bond next to the same protofilament as the

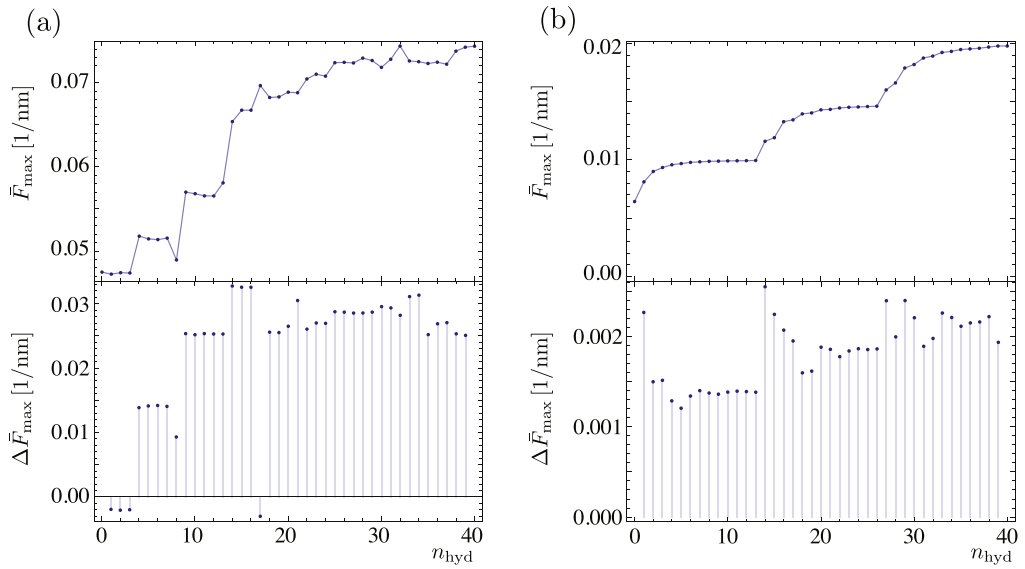

Figure 9. Random hydrolysis: maximal lateral bond force $\bar{F}_{\max} = F_{\max}/\kappa$ and change $\Delta\bar{F}_{\max}$ in the maximal lateral bond force after rupture of the maximally strained bond as a function of the number n_{hyd} of hydrolyzed GTP-dimers. We start with a MT with a three layer GTP-cap. (a) Strong lateral bond springs, $k/\kappa = 0.5\ \mathrm{nm}^{-2}$, and (b) weak lateral bond springs, $k/\kappa = 0.005\ \mathrm{nm}^{-2}$. The location of the lateral bond under maximal force within the GTP-cap is shown in figures 5 and 6 for strong and weak bonds, respectively, as thick black line.

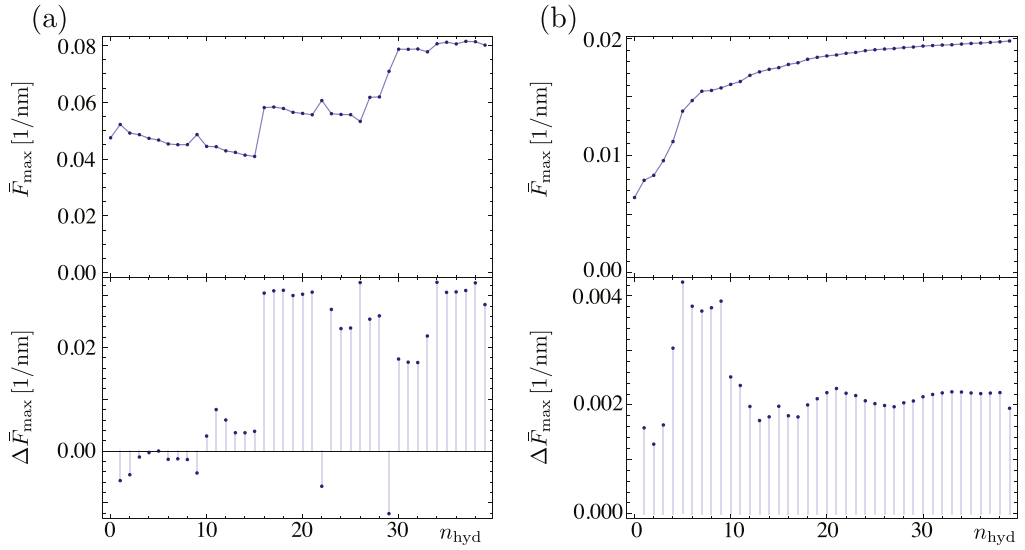

Figure 10. Vectorial hydrolysis: maximal lateral bond force $\bar{F}_{\max} = F_{\max}/\kappa$ and change $\Delta\bar{F}_{\max}$ in the maximal lateral bond force after rupture of the maximally strained bond as a function of the number n_{hyd} of hydrolyzed GTP-dimers. We start with a MT with a three layer GTP-cap. (a) Strong lateral bond springs, $k/\kappa = 0.5\ \mathrm{nm}^{-2}$, and (b) weak lateral bond springs, $k/\kappa = 0.005\ \mathrm{nm}^{-2}$. The location of the lateral bond under maximal force within the GTP-cap is shown in figures 7 and 8 for strong and weak bonds, respectively, as thick black line.

hydrolyzed dimer. Hydrolysis of the first dimer in a layer increases the spontaneous curvature of that protofilament and, thus, increases the strain on lateral bonds of the same protofilament in the last layer.

For vectorial hydrolysis, only dimers at the GTP-GDP interface can be hydrolyzed, and hydrolysis has to advance from the minus end side. The results for vectorial hydrolysis and strong lateral bonds, see figure 10(a), show that after hydrolysis of $n_{\mathrm{hyd}} = 16$ dimers, when the third protofilament becomes completely hydrolyzed, there is a pronounced step-like increase in $F_{\max}$. Similarly, for weak lateral bonds, see figure 10(b), there is a strong increase after hydrolysis of $n_{\mathrm{hyd}} = 5$ dimers, when the first protofilament becomes completely hydrolyzed. A completely hydrolyzed protofilament prefers to assume its curved equilibrium state and, thus, exerts strong outward forces on neighboring stabilizing protofilaments with GTP-caps. Therefore, with each completely hydrolyzed protofilament the strain on the lateral bonds increases. For weak bonds a single hydrolyzed protofilament is sufficient to cause a pronounced increase in $F_{\max}$, whereas for strong bonds several hydrolyzed protofilaments seem to be necessary. In the corresponding figures 7 for

strong lateral bonds and 8 for weak lateral bonds the location of the maximally strained lateral bond is shown as thick black line: the bond under maximal force occurs at the last layer of the cap next to the completely hydrolyzed protofilaments.

Typical values for $F_{\max}$ depend on the strength of lateral bonds. For strong lateral bonds ($k/\kappa = 0.5\ \mathrm{nm}^{-2}$) we find $F_{\max}/\kappa \sim 0.06\ \mathrm{nm}^{-1}$ both for random and vectorial hydrolysis. For $\kappa \sim 25\, k_BT$ well within the considered range $14k_BT \leqslant \kappa \ll 68k_BT$ of dimer bending rigidities, this gives maximal forces $F_{\max} \sim 6\mathrm{pN}$. For weak lateral bonds $\left(k/\kappa = 0.005\ \mathrm{nm}^{-2}\right)$ we find smaller maximal forces $F_{\max}/\kappa \sim 0.01\ \mathrm{nm}^{-1}$ corresponding to $F_{\max} \sim 1\mathrm{pN}$, which are again similar for random and vectorial hydrolysis.

3.2.2. Bond rupture and catastrophe initiation. To further characterize the susceptibility to a mechanical instability, i.e., a rupture avalanche as it happens in catastrophes, we also investigated the *change* $\Delta F_{\max}$ in the maximal lateral bond force if we rupture the maximally strained bond and calculate the new maximal lateral bond force on an intact bond, see the lower plots in figure 9 for random hydrolysis and figure 10 for vectorial hydrolysis. If $\Delta F_{\max}$ is large and positive, there is an increase in the maximal bond force and the possibility of an instability: a rupture force $F_{\mathrm{rup}} < F_{\max}$ below this maximal force level can give rise to continued bond rupture. Vice versa, a negative value for $\Delta F_{\max}$ signals a mechanical stable situation. Remarkably, we find a strong correlation between the pronounced increase in $F_{\max}$ and a pronounced increase in $\Delta F_{\max}$ to larger positive values, see figure 9 for random hydrolysis and figure 10 for vectorial hydrolysis.

This suggests that the pronounced increase in the maximal lateral bond force is the starting point of a catastrophe-like rupture avalanche, if we choose the value for the rupture force F_{rup} such that after the increase in $F_{\max}$, the maximal lateral bond force exceeds the rupture threshold. Using this criterion, a reasonable value for the rupture force for random hydrolysis is $F_{\mathrm{rup}} \sim 0.062\kappa\ \mathrm{nm}^{-1}$ for strong lateral bonds and $F_{\mathrm{rup}} \sim 0.011\kappa\ \mathrm{nm}^{-1}$ for weak lateral bonds. For vectorial hydrolysis, this suggests rupture forces $F_{\mathrm{rup}} \sim 0.055\kappa\ \mathrm{nm}^{-1}$ for strong lateral bonds and $F_{\mathrm{rup}} \sim 0.0125\kappa\ \mathrm{nm}^{-1}$ for weak lateral bonds. With values of $\kappa \sim 25k_BT$ from the range $14k_BT \leqslant \kappa \ll 68k_BT$ according to the bounds (14) and (15), the resulting rupture forces are $F_{\mathrm{rup}} \sim 5 - 6\mathrm{pN}$ for strong bonds or $1.2 - 1.3\mathrm{pN}$ for weak bonds, respectively.

We test whether our model exhibits catastrophe-like events if we fix a value for the rupture force according to this criterion by including bond rupture into our algorithm for the most probable hydrolysis pathway. After each hydrolysis step we check whether any lateral bond spring is loaded by a force larger than the rupture force. If this is the case, we rupture the corresponding spring by cutting it and mechanically relax the MT lattice. Then we test again for bond rupture and so on. If no further rupture events occur, we continue with the next hydrolysis step.

Using this simulation procedure we indeed find catastrophe events with continued bond rupture similar to

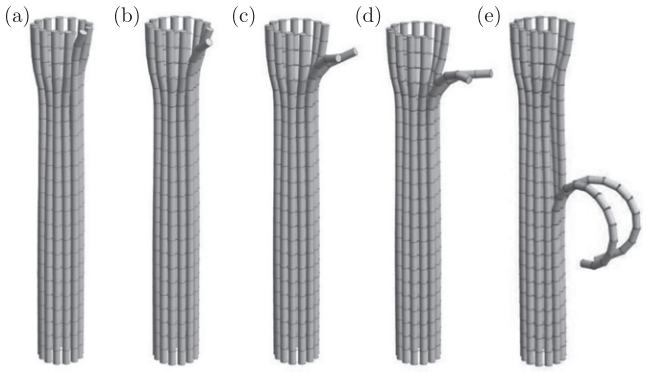

Figure 11. Catastrophe event for vectorial hydrolysis and weak lateral bond springs $k/\kappa = 0.005\ \mathrm{nm}^{-2}$ using a rupture force $F_{\mathrm{rup}} = 0.0125\kappa\ \mathrm{nm}^{-1}$ ($m_1 = 20$ and $m_2 = 3$). The numbers n_{hyd} of hydrolyzed dimers and n_{cut} of cut lateral bonds are (a) $n_{\mathrm{hyd}} = 5$, $n_{\mathrm{cut}} = 1$, (b) $n_{\mathrm{hyd}} = 6$, $n_{\mathrm{cut}} = 4$, (c) $n_{\mathrm{hyd}} = 6$, $n_{\mathrm{cut}} = 8$, (d) $n_{\mathrm{hyd}} = 6$, $n_{\mathrm{cut}} = 11$, (e) $n_{\mathrm{hyd}} = 6$, $n_{\mathrm{cut}} = 33$.

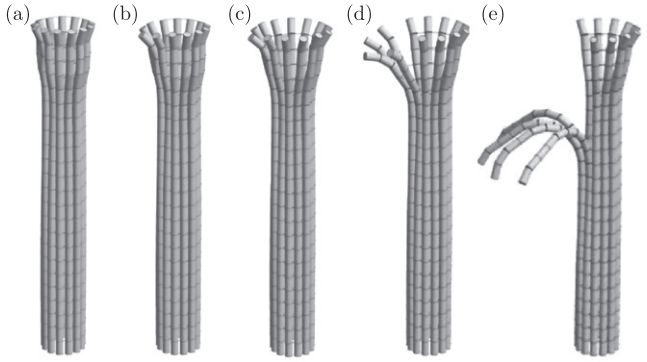

Figure 12. Catastrophe event for random hydrolysis and weak lateral bond springs $k/\kappa = 0.005\ \mathrm{nm}^{-2}$ using a rupture force $F_{\mathrm{rup}} = 0.011\kappa\ \mathrm{nm}^{-1}$ ($m_1 = 20$ and $m_2 = 3$). The numbers n_{hyd} of hydrolyzed dimers and n_{cut} of cut lateral bonds are (a) $n_{\mathrm{hyd}} = 14$, $n_{\mathrm{cut}} = 1$, (b) $n_{\mathrm{hyd}} = 14$, $n_{\mathrm{cut}} = 6$, (c) $n_{\mathrm{hyd}} = 14$, $n_{\mathrm{cut}} = 15$, (d) $n_{\mathrm{hyd}} = 14$, $n_{\mathrm{cut}} = 24$, (e) $n_{\mathrm{hyd}} = 14$, $n_{\mathrm{cut}} = 45$.

experimentally observed catastrophes. For vectorial hydrolysis, see figure 11, typically single protofilaments peel off the MT lattice and curl into 'ram's horn' conformations. During all the rupture events shown in figure 11, we have $n_{\mathrm{hyd}} = 5$ or 6, i.e., hydrolysis practically stops during such an event. The hydrolysis state at $n_{\mathrm{hyd}} = 5$ consists of a single completely hydrolyzed protofilament (see figure 8). Therefore, the initial stress distribution in lateral bonds is concentrated on this protofilament. The stress due to the preferred curved configuration of this protofilament triggers the bond rupture of neighboring lateral bonds, and this protofilament starts to peel off during the catastrophe.

For random hydrolysis, see figure 12, typically several protofilaments peel off the MT lattice. Also for this hydrolysis mechanism, the hydrolysis stops during such an event: the entire catastrophe event in figure 12 happens at $n_{\mathrm{hyd}} = 14$. For random hydrolysis the stress is typically distributed among the entire top layer of lateral bonds because mechanically

dominated hydrolysis proceeds layer by layer; the state $n_{\mathrm{hyd}} = 14$ consists of a completely hydrolyzed plus end layer of dimers with one additional hydrolysis event in the next layer, see figure 6. This gives rise to several bond rupture events within the top layer and several protofilaments peeling off the MT.

These different catastrophe characteristics for vectorial and random hydrolysis could be an interesting issue for future experimental studies.

4. Discussion and conclusion

We introduced a mechanical model, which gives stable tubular MT structures if a stabilizing GTP-cap is present in accordance with experimental observations. The model includes intra-dimer bending and one lateral bond per dimer. In order to avoid overlapping of tubulin dimers we also include a sufficiently strong hard core interaction. We use the allosteric model for the hydrolysis state of tubulin dimers: GTP dimers are straight; after hydrolysis, a GDP dimer has an equilibrium bending angle of 22°.

We obtained several constraints for the model parameters, the bending rigidity κ and the lateral bond strength k: (i) The ratio k/κ is constrained by a lower bound $k/\kappa \geqslant 0.001\ \mathrm{nm}^{-2}$, see (10), which ensures that GTP-capped MTs do not spontaneously acquire a strongly bent shape similar to the ram's horn configuration. (ii) The value for κ is constrained by an upper bound (14) because hydrolysis is not observed to be a reversible reaction and the free energy released in hydrolysis should exceed the mechanical energy increase in the MT lattice during hydrolysis. (iii) If we additionally assume that hydrolysis is dominated by mechanical forces in the MT lattice, i.e., typical mechanical energy changes of the the MT lattice during hydrolysis exceed the thermal energy k_BT, the value for κ is also constrained by a lower bound (15). The bounds (ii) and (iii) define a range $14k_BT \leqslant \kappa \ll 68k_BT$ of dimer bending rigidities.

The mechanical model allows us to investigate the interplay of mechanical forces in the MT lattice and hydrolysis, which has not been done previously. The interaction via the mechanics of the MT lattice can give rise to possible correlation effects in the hydrolysis dynamics, which have not been taken into account before. Under the assumption of a mechanically dominated hydrolysis reaction the concept of a *most probable hydrolysis pathway* becomes very useful. We calculated most probable hydrolysis pathways numerically both for random hydrolysis (figures 5 and 6), where all GTP-dimers in the MT cap can be hydrolyzed, and for vectorial hydrolysis (figures 7 and 8), where only GTP-dimers at the GTP-GDP interface can be hydrolyzed. We also studied the effect of lateral bond strength on the hydrolysis pathway.

For mechanically dominated random hydrolysis, the most probable hydrolysis pathway shows a preference for layer-by-layer hydrolysis starting at the GTP-layer at the plus end. For mechanically dominated vectorial hydrolysis, the most probable hydrolysis pathway shows a preference for hydrolysing complete protofilaments towards the plus end starting from a certain 'nucleus' configuration consisting of three neighboring hydrolyzed GDP-dimers within the same layer. This could be related to the experimental observation of several rate-limiting steps for catastrophe initiation [14].

We also investigated the lateral bond forces occurring during hydrolysis. For random hydrolysis, mechanically dominated hydrolysis proceeds in a layer-by-layer fashion starting at the plus end, and we found sharp increases of the maximal lateral bond force if hydrolysis of one layer has been completed and hydrolysis of the next layer starts. The respective maximal forces occur at the plus end of the MT. For vectorial hydrolysis and weak lateral bonds, we found a sharp increase of the maximal lateral bond force if a single protofilament becomes completely hydrolyzed. For stronger lateral bonds, several protofilaments need to become completely hydrolyzed to trigger a similar increase in the maximal lateral bond force. The respective maximal forces occur right at the plus end.

Moreover, we observe that the MT lattice becomes mechanically unstable at the sharp increase: rupture of the maximally strained bond further *increases* the maximal bond force, which signals an instability with respect to a catastrophe event initiated by lateral bond rupture. If the rupture force value lies within the force range set by the sharp increase of the maximal lateral bond force, we indeed find continued bond rupture and catastrophe events as observed in experiments, see figures 11 and 12. Using this criterion we find rupture force values between 1pN for weak and 5pN for strong lateral bonds. For vectorial hydrolysis, we find catastrophes starting with single protofilaments peeling off the MT. For random hydrolysis, on the other hand, we typically see several protofilaments peeling off the MT. These characteristic differences in our simulations could motivate further experimental studies of this issue.

Our results suggest several routes for future work. Firstly, we only studied MTs of fixed length for simplicity. Further investigations will include stochastic polymerization and depolymerization similar to the models in [30, 43]. Secondly, we assumed so far that hydrolysis is mechanically dominated and forces on the most probable hydrolysis pathway by selecting the next GTP-dimer to be hydrolyzed according to the maximal mechanical energy gain. Future models should be fully stochastic with hydrolysis rates *modulated* by mechanical energies in order to include all hydrolysis pathways with their respective statistical weight into the analysis. Finally, a similar mechanical MT model and its coupling to hydrolysis should be investigated not only for the allosteric model but also for the lattice model of dimer hydrolysis.

Acknowledgments

We thank Björn Zelinski and Sebastian Knoche for fruitful discussions, and we acknowledge support by the Deutsche Forschungsgemeinschaft (KI 662/4-1).

References

[1] Mitchison T J and Salmon E D 2001 *Nat. Cell Biol.* **3** 17–21
[2] Dogterom M, Kerssemakers J W J, Romet-Lemonne G and Janson M E 2005 *Curr. Opin. Cell Biol.* **17** 67–74
[3] Daga R R, Yonetani A and Chang F 2006 *Curr. Biol.* **16** 1544–50
[4] Siegrist S E and Doe C Q 2007 *Genes Dev.* **21** 483–96
[5] Picone R, Ren X, Ivanovitch K D, Clarke J D W, McKendry R A and Baum B 2010 *PLoS Biol.* **8** e1000542
[6] Dehmelt L, Smart F M, Ozer R S and Halpain S 2003 *J. Neurosci.* **23** 9479–90
[7] Mitchison T and Kirschner M 1984 *Nature* **312** 237–42
[8] Kirschner M, Williams R, Weingarten M and Gerhart J C 1974 *Proc. Natl. Acad. Sci. USA* **71** 1159–63
[9] Wang H and Nogales E 2005 *Nature* **435** 911–5
[10] Buey R, Diaz J and Adreu J 2006 *Biochemistry* **45** 5933–8
[11] Wu Z, Nogales E and Xing J 2012 *Biophys. J.* **102** 2687–96
[12] Nogales E and Wang H 2006 *Curr. Opin. Struct. Biol.* **16** 221–9
[13] Müller-Reichert T, Chrétien D, Severin F and Hyman A A 1998 *Proc. Natl. Acad. Sci. USA* **95** 3661–6
[14] Gardner M K, Zanic M, Gell C, Bormuth V and Howard J 2011 *Cell* **147** 1092–103
[15] Van Doorn G, Tanase C, Mulder B M and Dogterom M 2000 *Eur. Biophys. J.* **29** 2–6
[16] Kolomeisky A B and Fisher M 2001 *Biophys. J.* **80** 149–54
[17] Stukalin E B and Kolomeisky A B 2004 *J. Chem. Phys.* **121** 1097–104
[18] Ranjith P, Lacoste D, Mallick K and Joanny J-F 2009 *Biophys. J.* **96** 2146–59
[19] Krawczyk J and Kierfeld J 2011 *EPL* **93** 28006
[20] Dogterom M and Leibler S 1993 *Phys. Rev. Lett.* **70** 1347–50
[21] Flyvbjerg H, Holy T and Leibler S 1994 *Phys. Rev. Lett.* **73** 2372–5
[22] Flyvbjerg H, Holy T and Leibler S 1996 *Phys. Rev.* E **54** 5538–60
[23] Zelinski B, Müller N and Kierfeld J 2012 *Phys. Rev.* E **86** 041918
[24] Zelinski B and Kierfeld J 2013 *Phys. Rev.* E **87** 012703
[25] Sept D and MacKintosh F C 2010 *Phys. Rev. Lett.* **104** 018101
[26] Wells D B and Aksimentiev A 2010 *Biophys. J.* **99** 629–37
[27] Grafmüller A and Voth G 2011 *Structure* **19** 409–17
[28] Grafmüller A, Noya E G and Voth G 2013 *J. Mol. Biol.* **425** 2232–46
[29] Bayley P M, Schilstra M J and Martin S R 1990 *J. Cell Sci.* **95** 33–48
[30] VanBuren V, Odde D J and Cassimeris L 2002 *Proc. Natl. Acad. Sci. USA* **99** 6035–40
[31] Brun L, Rupp B, Ward J J and Nédélec F 2009 *Proc. Natl. Acad. Sci. USA* **106** 21173–8
[32] Bowne-Anderson H, Zanic M, Kauer M and Howard J 2013 *Bioessays* **35** 452–61
[33] Jemseena V and Gopalakrishnan M 2013 *Phys. Rev.* E **88** 032717
[34] Padinhateeri R, Kolomeisky A B and Lacoste D 2012 *Biophys. J.* **102** 1274–83
[35] Li X L and Kolmeisky A B 2013 *J. Phys. Chem.* B **117** 9217–23
[36] Li X, Kierfeld J and Lipowsky R 2009 *Phys. Rev. Lett.* **103** 048102
[37] Li X, Lipowsky R and Kierfeld J 2010 *EPL* **89** 38010
[38] Drechsel D and Kirshner M 1994 *Curr. Biol.* **4** 1053–61
[39] Desai A and Mitchison T J 1997 *Annu. Rev. Cell Dev. Biol.* **13** 83–117
[40] Schek H T, Gardner M K, Cheng J, Odde D J and Hunt A J 2007 *Curr. Biol.* **17** 1445–55
[41] Molodtsov M I, Ermakova A E, Shnol E E, Grishchuk E L, McIntosh J R and Ataullakhanov F I 2005 *Biophys. J.* **88** 3167–79
[42] Mohrbach H, Johner A and Kulić I M 2010 *Phys. Rev. Lett.* **105** 268102
[43] VanBuren V, Cassimeris L and Odde D J 2005 *Biophys. J.* **89** 2911–26
[44] Carlier M F, Didry D and Pantaloni S 1987 *Biochemistry* **26** 4428–37
[45] Nogales E 2000 *Annu. Rev. Biochem.* **69** 277–302
[46] Kis A, Kasas S, Kulik A J, Catsicas S and Forro L 2008 *Langmuir* **24** 6176–81
[47] Molodtsov M I, Grishchuk E L, McIntosh J R and Ataullakhanov F I 2005 *Proc. Natl. Acad. Sci. USA* **102** 4353–8
[48] Pampaloni F, Lattanzi G, Jonas A, Surrey T, Frey E and Florin E L 2006 *Proc. Natl. Acad. Sci. USA* **103** 10248–53
[49] Bell G I 1978 *Science* **200** 618–27